PENGUIn/AGO and THEMIS conjugate observations of whistler mode chorus waves in the dayside uniform zone under steady solar wind and quiet geomagnetic conditions

Kunihiro Keika,[1] Maria Spasojevic,[2] Wen Li,[3] Jacob Bortnik,[3] Yoshizumi Miyoshi,[4] and Vassilis Angelopoulos[5]

Received 12 March 2012; revised 12 May 2012; accepted 28 May 2012; published 18 July 2012.

[1] We perform a case study of conjugate observations of whistler mode chorus waves on the dayside made on 26 July 2008 by three THEMIS spacecraft and ground-based ELF/VLF receivers at the Automatic Geophysical Observatories (AGO) in Antarctica supported by the U.S. Polar Experiment Network for Geospace Upper-atmosphere Investigations (PENGUIn) project. The dayside chorus waves were excited during a period of no substorm activity with geomagnetic indices indicating quiet conditions (Dst ~ -10 nT; AE < 200 nT). The solar wind dynamic pressure was almost constant during the chorus wave intensification. Conjugate observations in the outer magnetosphere confirm that the chorus intensification was localized within the radial distance R = 7–10 R_E near noon (12.5 < MLT < 13.5 h). The waves persisted for at least 1.5 h in the same location, where field lines are not accompanied by off-equatorial minimum-B pockets but rather exhibit nearly zero dB/ds, the field-aligned gradient in B-magnitude, over a wide range of magnetic latitudes ($\sim\pm20^\circ$). The location did not seem to corotate with the Earth or drift with the energetic electrons. The chorus waves consisted of discrete, rising tone elements, propagating away from the magnetic equator, quasi-parallel to the ambient magnetic field (wave-normal angles < 20°). We conclude that the long-lasting, localized, quiet time dayside chorus amplification was due to the nearly zero dB/ds conditions that occur naturally in the dayside uniform zone (DUZ), the transition region between the near-Earth dipole and the compressed, off-equatorial double-minimum field configuration found closer to the magnetopause. We thus suggest that the magnetic field configuration in the dayside outer magnetosphere plays a key role in the generation of dayside chorus waves under quiet geomagnetic conditions.

Citation: Keika, K., M. Spasojevic, W. Li, J. Bortnik, Y. Miyoshi, and V. Angelopoulos (2012), PENGUIn/AGO and THEMIS conjugate observations of whistler mode chorus waves in the dayside uniform zone under steady solar wind and quiet geomagnetic conditions, *J. Geophys. Res.*, *117*, A07212, doi:10.1029/2012JA017708.

1. Introduction

[2] Chorus waves are electromagnetic emissions characterized by a sequence of discrete elements typically in the range of 0.1–0.8 f_{ce} [e.g., *Sazhin and Hayakawa*, 1992; *Meredith et al.*, 2001a; *Parrot et al.*, 2003b; *Bortnik et al.*, 2008; *Kasahara et al.*, 2009; *Meredith et al.*, 2009; *Omura et al.*, 2009; *Haque et al.*, 2010; *Hayosh et al.*, 2010; *Macúšová et al.*, 2010; *Schriver et al.*, 2010; *Santolík et al.*, 2010a, 2010b; *Li et al.*, 2011b, 2011c], where f_{ce} is the equatorial electron cyclotron frequency. These emissions typically occur in two frequency bands, a lower band (0.1–0.5 f_{ce}) and an upper band (0.5–0.8 f_{ce}) with a gap at 0.5 f_{ce} [e.g., *Burtis and Helliwell*, 1969; *Sazhin and Hayakawa*, 1992; *Bell et al.*, 2009; *Omura et al.*, 2009]. Chorus waves are excited through the electron cyclotron instability by anisotropic distributions of energetic electrons with energies of ~1–100 keV and subsequent nonlinear process [e.g., *Kennel and Petschek*, 1966; *Omura et al.*, 2008] although

[1]Center for Solar Terrestrial Research, New Jersey Institute of Technology, Newark, New Jersey, USA.
[2]Space Telecommunications and Radioscience Laboratory, Stanford University, Palo Alto, California, USA.
[3]Department of Atmospheric and Oceanic Sciences, University of California, Los Angeles, California, USA.
[4]Solar-Terrestrial Environment Laboratory, Nagoya University, Nagoya, Japan.
[5]Institute of Geophysics and Planetary Physics, Department of Earth and Space Sciences, University of California, Los Angeles, California, USA.

Corresponding author: K. Keika, Center for Solar Terrestrial Research, New Jersey Institute of Technology, Newark, NJ 07102, USA. (keika@adm.njit.edu)

0148-0227/12/2012JA017708

the details of the generation process are still under investigation [*Schriver et al.*, 2010; *Santolík et al.*, 2010b; *Omura and Nunn*, 2011].

[3] Chorus waves observed on the nightside are frequently associated with substorms or enhanced convection, due to mid-energy electrons freshly generated/injected [e.g., *Abel et al.*, 2006; *Miyoshi et al.*, 2007; *Li et al.*, 2009] and strongly heated adiabatically. The heating perpendicular to the local magnetic field results in anisotropic pitch angle distributions and temperature anisotropy, which are unstable to wave growth. The night-side chorus waves are observed mostly under disturbed geomagnetic conditions [*Tsurutani and Smith*, 1974; *Meredith et al.*, 2001b; *Miyoshi et al.*, 2003; *Li et al.*, 2011a] and are narrowly confined to around the magnetic equator (within 5–10° MLAT) [e.g., *LeDocq et al.*, 1998; *Parrot et al.*, 2003a; *Bortnik et al.*, 2007b; *Sigsbee et al.*, 2010; *Bunch et al.*, 2011].

[4] Chorus waves on the dayside, on the other hand, have a relatively high overall occurrence probability compared with other magnetospheric regions [*Tsurutani and Smith*, 1977; *Sigsbee et al.*, 2010; *Li et al.*, 2011a] and show little dependence of occurrence on geomagnetic activity [*Tsurutani and Smith*, 1977; *Spasojević and Inan*, 2010]. Dayside chorus has been observed over a wider range of magnetic latitudes (extending at least 25° off the equator) [e.g., *Burton and Holzer*, 1974; *Tsurutani and Smith*, 1977; *Meredith et al.*, 2001a; *Vaivads et al.*, 2007; *Tsurutani et al.*, 2009]. *Tsurutani and Smith* [1977] reported chorus emissions on the dayside at magnetic latitudes of ≥15° and within a few R_E of the magnetopause. *Vaivads et al.* [2007] reported a case of dayside chorus generation at a local minimum of the magnetic field off the magnetic equator. *Tsurutani et al.* [2009] demonstrated two dayside chorus events during which the Poynting flux was directed toward the equator, suggesting that the chorus waves were generated and grown near the minimum-B pockets. Measurements by the Polar spacecraft showed intense chorus waves at high latitudes on the dayside [*Sigsbee et al.*, 2010; *Bunch et al.*, 2011] and a chorus population propagating toward the equator [*Santolík et al.*, 2010b]. *Bunch et al.* [2012] showed that the time-averaged chorus wave power in the dayside outer magnetosphere can exceed 10 pT for latitudes up to 45° off the equator.

[5] Such unique characteristics of dayside chorus may be explained by the distortion of the dayside magnetospheric configuration caused by solar wind compression. The day-night asymmetry of the magnetosphere due to this distortion results in a so-called drift shell splitting effect, whereby, drift paths of energetic electrons (i.e., the source population of chorus wave generation) are pitch angle dependent [*Roederer*, 1967, 1970; *West et al.*, 1973; *Schulz and Lanzerotti*, 1974; *Sibeck et al.*, 1987; *Takahashi et al.*, 1997; *Min et al.*, 2010]. As electrons drift from the nightside toward the dayside, electrons with small equatorial pitch angles (α_{eq}) drift at smaller radial distances than those with $\alpha_{eq} \sim 90°$. This effect could cause more $\alpha_{eq} \sim 90°$ electrons and less electrons with $\alpha_{eq} \sim 0°$ or 180° to reach the dayside outer magnetosphere, leading to pancake-like distributions which enhance the linear growth of chorus waves there.

[6] The distorted configuration also provides two minima of the magnetic field strength at high latitudes near the dayside magnetopause, one of which is in the northern hemisphere and the other in the southern hemisphere. Under this configuration, energetic electrons with $\alpha_{eq} \sim 90°$ do not follow equatorial isomagnetic contours but move along one of the two branches of the minimum *B* points (through so-called Shabansky orbits). This drift motion is called drift shell bifurcation [e.g., *Shabansky*, 1971; *Öztürk and Wolf*, 2007; *Kim et al.*, 2008; *Saito et al.*, 2010; *Ukhorskiy et al.*, 2011], which could give rise to high electron flux and/or anisotropic distributions near off-equatorial minimum *B* pockets.

[7] In addition, the distorted dayside configuration produces a region of quasi-uniform field lines around the magnetic equator. In the transition region from a dipolar configuration in the inner magnetosphere to the off-equatorial double minimum-*B* configuration near the dayside magnetopause, the gradient of the magnetic field strength along the field line (*dB*/*ds*) becomes nearly zero for a long distance around the equator. Smaller *dB/ds* enhances the force of the waves on the electrons relative to the adiabatic forces, thus increasing the probability of phase-trapping of electrons in the potential well of the wave, which is considered a necessary condition for nonlinear wave growth [*Nunn*, 1974; *Dowden et al.*, 1978; *Bell and Inan*, 1981; *Omura et al.*, 1991].

[8] Dayside chorus generation may also be associated with ULF waves. A large number of studies have reported and analyzed modulation of tens to hundreds of keV electron flux by ULF waves in the Pc5 frequency band [e.g., *Kimura*, 1974; *Kokubun et al.*, 1977; *Kremser et al.*, 1981; *Nosé et al.*, 1998; *Kleimenova et al.*, 2005; *Spanswick et al.*, 2005; *Sarris et al.*, 2007; *Manninen et al.*, 2010]. Since such energetic electrons are the free energy source of the chorus waves, it is probable that the ULF modulation affects the growth rate of chorus waves and in turn causes wave generation. Recently, *Li et al.* [2011c] reported with THEMIS data a clear correlation between ULF pulsation and chorus wave modulation.

[9] Scattering of energetic electrons due to magnetospheric waves followed by precipitation into the atmosphere causes pancake-like distributions to remain in the equatorial magnetosphere [*Wrenn et al.*, 1979; *Horne and Thorne*, 2000; *Meredith et al.*, 2000; *Su et al.*, 2009; *Thorne et al.*, 2010; *Tao et al.*, 2011], providing an increase in electron anisotropy. Since the scattering takes place as electrons drift eastward from the nightside toward the dayside, the scattering process may play an important role in electron anisotropy increases, which ultimately generate chorus waves on the dayside.

[10] Dayside whistler mode chorus is at times related to sudden enhancements of the solar wind dynamic pressure. It has been reported that a sudden magnetospheric compression triggers chorus or increases its intensity [*Gail and Inan*, 1990; *Gail et al.*, 1990; *Salvati et al.*, 2000; *Fu et al.*, 2012]. This type of dayside chorus is attributed to compression-related adiabatic heating leading to electron anisotropy and thus increases in the chorus wave growth rate.

[11] In this paper, we examine a dayside chorus event that occurred on 26 July 2008, under quiet geomagnetic conditions with no substorm activity, in a steady state magnetosphere. We use ELF/VLF data from conjugate observations by three spacecraft of the Time History of Events and

Macroscale Interactions During Substorms (THEMIS) mission [*Angelopoulos*, 2008] and at the Automatic Geophysical Observatories (AGO) in Antarctica supported by the U.S. Polar Experiment Network for Geospace Upper-atmosphere Investigations (PENGUIn) project [*Lessard et al.*, 2009; *Mende et al.*, 2009], both of which provide high-resolution power spectrograms of ELF/VLF waves. After introducing the data set in Section 2, we present solar wind and geomagnetic conditions during the event in Section 3, ELF/VLF wave observations at AGO-AP2 station in Section 4, and THEMIS observations in Section 5. In Section 6, using the Tsyganenko magnetic field model, we examine the configuration of the dayside magnetosphere during the event. The observations indicate that the chorus wave intensification persisted for at least 1.5 h in the same location. The long-lasting and localized intensification occurred on field lines that exhibit smaller field-aligned gradient in *B*-magnitude than the dipole field. The results of the observations and analyses are summarized and discussed in Section 7, followed by our conclusions in Section 8.

2. Data Set

2.1. ELF/VLF Data From AGO Stations

[12] AGO stations are powered with wind generators and solar panels; data from these stations are transmitted to the U.S. via Iridium modems continuously throughout the year. The observatories for which data are available for the event examined in this study, AP2, SPA, and AP1 are located along a magnetic meridian delineated by the geomagnetic and geographic South Poles; the CGM latitude and longitude at 100 km reference are (−69.81°, E19.21°) for AP2, (−74.02°, E18.35°) for SPA, and (−80.14°, E16.75°) for AP1, and the difference between UT and MLT is MLT = UT − 3.5 h.

[13] ELF/VLF receivers at the AGO sites record wave activity incident upon orthogonal loop antennas in multiple frequency-banded channels as well as in broadband snapshots [*Salvati et al.*, 2000; *Spasojević and Inan*, 2010]. The system records the average amplitude in a set of band-pass filtered frequency channels (0.5–40 kHz) twice per second. The system also records full waveform data up to 4.5 kHz every 5 min; the recording is made for 2 s.

2.2. THEMIS Data

[14] The THEMIS spacecraft, which consist of five identical probes, were launched on 17 February 2007 in near-equatorial orbits [*Angelopoulos*, 2008]. In July 2008, the perigee and apogee were ∼1.5 and ∼10 R_E for THEMIS A, ∼1.5 and ∼12 R_E for THEMIS D and E, ∼1.2 and ∼20 R_E for THEMIS C, and ∼1.3 and ∼30 R_E for THEMIS B. The orbital period was ∼1 day for THEMIS A, D, and E, ∼2 days for THEMIS C, and ∼4 days for THEMIS B.

[15] ELF/VLF waves can be detected by the Search-Coil Magnetometer (SCM) [*Le Contel et al.*, 2008; *Roux et al.*, 2008] and the Electric Field Instrument (EFI) [*Bonnell et al.*, 2008]. SCM and EFI measure waves in a frequency range from 0.1 Hz to 4 kHz and up to 8 kHz, respectively. The SCM and EFI output waveforms are processed by the Digital Fields Board (DFB) [*Cully et al.*, 2008]. The amplitude of the magnetic and electric fields in the spin plane is filtered through multiple passbands and stored as filter bank data, which thus contain 4-s wave amplitude data in six logarithmically spaced frequency bands in a range of ∼2 Hz to 4 kHz.

[16] An orbit's data collection is apportioned to the Fast or Slow Survey instrument mode operations. During both types of survey, filter bank data are collected routinely. Particle-Burst modes are interspersed six times within the Fast Survey collection interval, according to on-board triggers, in order to maximize particle data collection. Twice during each Particle-Burst interval, two Wave-Burst mode intervals provide maximum cadence field waveforms, up to 8000 or 16000 samples/second. Thus, 12 times per day per spacecraft it is possible to obtain high-fidelity cross-spectral products of the waves and perform wave mode identification by ground-processing. All Wave-Bursts are captured based on on-board wave power triggers.

[17] The Fluxgate Magnetometer (FGM) [*Auster et al.*, 2008] measures background magnetic fields and their low-frequency fluctuations (up to 64 Hz). FGM data in this study are utilized to evaluate local electron cyclotron frequencies in order to scale chorus frequencies.

[18] Electron pitch angle distributions are available from the Electro-Static Analyzer (ESA) [*McFadden et al.*, 2008] for energies between a few eV and 30 keV. The energy range covers key resonant energies to chorus wave generation, as demonstrated in statistical studies by *Li et al.* [2010].

[19] The total electron density is inferred from the spacecraft potential measured by EFI and electron thermal speed measured by ESA. The electron density outside the plasmapause is calibrated by a statistical comparison with 2 years of ESA observations for each spacecraft, while the plasmasphere density is estimated by fitting the statistical density profile given by *Sheeley et al.* [2001]. Details of the method are described by *Mozer* [1973] and *Pedersen et al.* [1998].

2.3. Conjugate Observations

[20] Figure 1 presents the relative locations of AGO stations used in this study and three THEMIS probes during the conjugate observations between 1230 and 1930 UT on 26 July 2008. Figure 1a shows a map of the AGO stations along with the viewing area of the ELF/VLF receiver at AP2 and THEMIS magnetic foot points. The ELF/VLF viewing area is defined as a 500 km circle at 100 km altitude around a station. Figure 1b presents THEMIS orbits projected onto the X-Y plane in SM coordinates along with the field-of-view (FOV) of the AP2 station. FOV is the ELF/VLF receiver viewing area mapped onto the X-Y plane; we use the Tsyganenko magnetic field model (TS01) [*Tsyganenko*, 2002a, 2002b] for mapping. Colored curved, closed lines drawn in Figure 1b are AP2 FOVs for specific UT hours.

[21] THEMIS A, D, and E traveled in an outbound path at R = 5.5–11 R_E and MLT = 11.5–13 h. Both THEMIS A and D were magnetically conjugate to AP2 between ∼1600 and ∼1700 UT and to AP3 between ∼1430 and ∼1530 UT. THEMIS E was conjugate to AP2 between ∼1530 and ∼1630 UT. This study uses ELF/VLF data from the AP2 station; burst-mode wave data, filter bank wave power

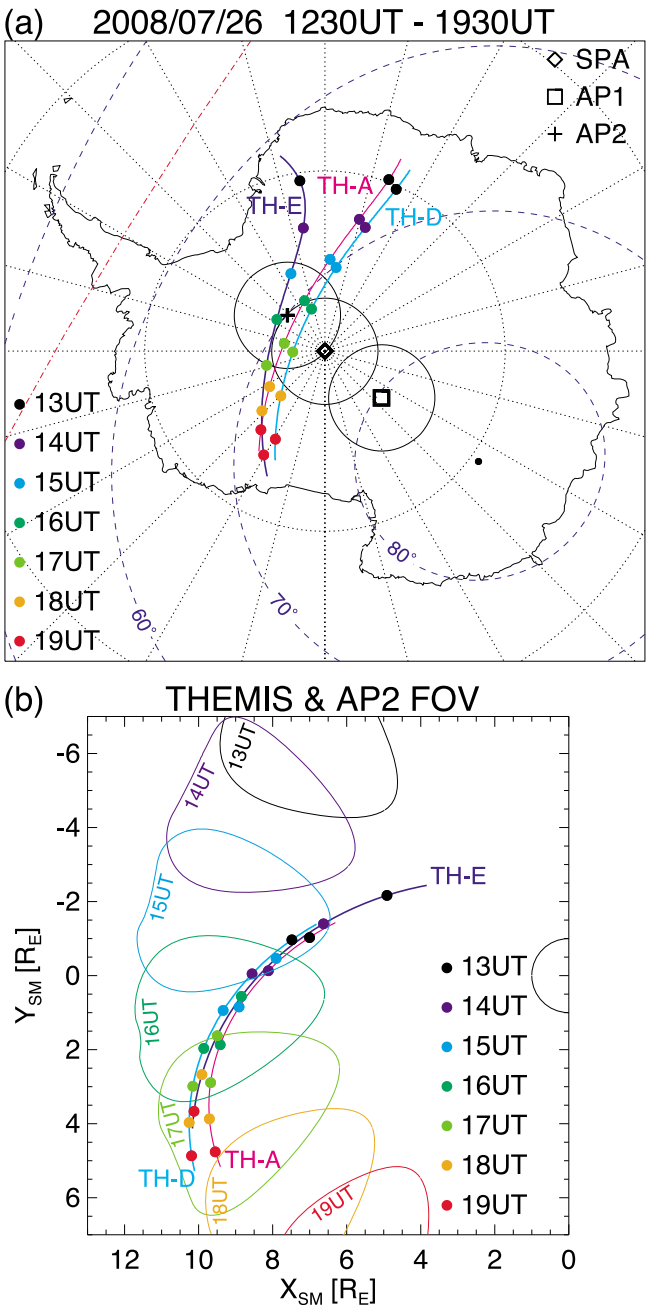

Figure 1. (a) A map of Antarctic observatories used in this study along with the trajectories of THEMIS magnetic foot points. Color of small solid circles on the trajectories indicate hours of 26 July 2008 in UT, listed near the left-bottom corner. The open circle around a station is the VLF receiver viewing area defined as a 500 km circle. The numbers in blue on the dashed curves show magnetic latitudes. The red dot-dashed line represents the day-night terminator at 16 UT. (b) THEMIS orbits in the X-Y plane in SM coordinates along with the field-of-views of the VLF receiver at the AP2 station mapped onto the X-Y plane for different UTs. Color of small solid circles on the THEMIS trajectories and FOVs indicate hours of 26 July 2008 in UT, listed near the right-bottom corner.

data, electron data, and spin-fit magnetic field data from THEMIS.

3. Observations on 26 July 2008

3.1. Solar Wind and Geomagnetic Conditions

[22] Figure 2 is a 1-day plot of solar wind data from the Wind spacecraft located at $(X, Y, Z)_{GSM} = (229, -93, 38)$ R_E at 1500 UT (Figures 2a and 2b), geomagnetic indices (Figures 2c and 2d), and magnetic field data from GOES spacecraft (Figures 2e and 2f) for 26 July 2008. The X_{GSM} and Y_{GSM} components of the interplanetary magnetic field (IMF) were predominantly negative and positive, respectively, for most of the interval. The Z_{GSM} component was fluctuating within ±5 nT. The solar wind dynamic pressure (P_d) was almost constant, near ~1 nPa, for the whole day.

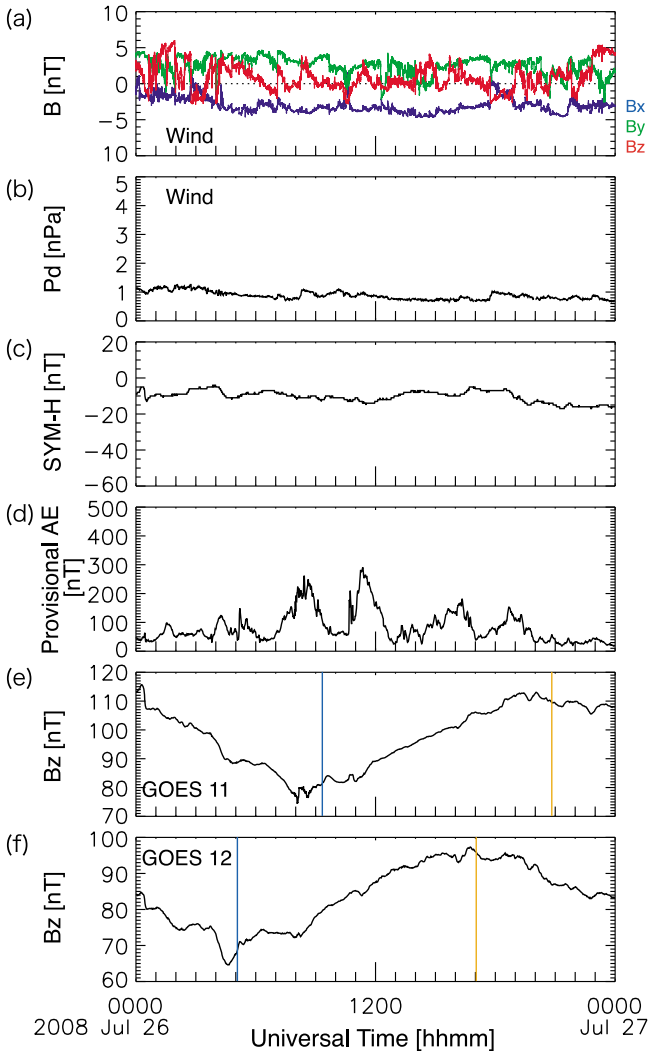

Figure 2. Time profile of (a) the three IMF components in GSM coordinates and (b) dynamic pressure of the solar wind obtained from the Wind spacecraft, (c) the SYM-H index, (d) the provisional AE index, and (e) the Z-component of the background magnetic field in SM coordinates observed by GOES 11 and (f) GOES 12 on 26 July 2008. Blue and orange vertical lines in Figures 2e and 2f represent the local midnight and noon, respectively.

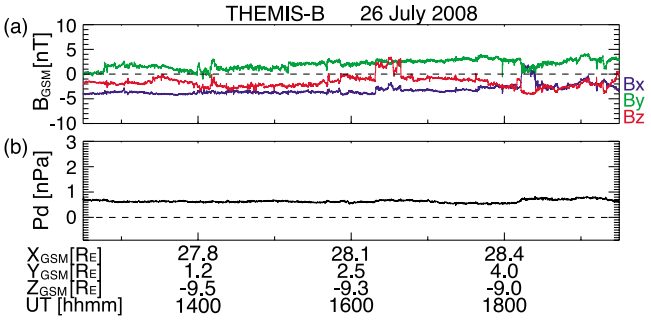

Figure 3. THEMIS B observations of (a) the three IMF components in GSM coordinates and (b) dynamic pressure of the solar wind between 1230 and 1930 UT on 26 July 2008.

The SYM-H index was between −20 and 0 nT, indicating that no geomagnetic storm occurred. The AE index was below 300 nT with two small substorm events of ∼300 nT peaking at 08–09 UT and 11–12 UT, that is, prior to the interval of interest.

[23] The Z_{SM} component of the magnetic field at GOES 11 and 12 shows typical diurnal variations with its maximum around local noon and its minimum around local midnight. GOES 11 observed a dipolarization at ∼8 UT. The dipolarization is associated with geomagnetic activity represented by the AE enhancement at 08–09 UT.

[24] Figure 3 presents IMF and P_d at THEMIS B upstream of the bow shock ($X_{GSM} \sim 28\ R_E$) between 1230 and 1930 UT. IMF was small, each component being within ±5 nT. A sudden change of IMF occurred at ∼1620 UT and ∼1815 UT. IMF Z_{GSM} component was negative except for a ∼20 min interval after the northward turning at ∼1620 UT. IMF fluctuations were small, ΔB is mostly less than 1 nT, P_d was almost constant at ∼0.7 nPa, and no sudden change was seen to occur.

[25] In summary, observations of the solar wind, geomagnetic indices, and the magnetic field at geosynchronous orbit indicate that the period of interest was very quiet with only small patches of occasional activity.

3.2. ELF/VLF Observations at PENGUIn/AGO P2 in Antarctica

[26] Figure 4a shows the temporal profile of ELF/VLF signals detected at the AP2 station between 1230 and 1930 UT. Shown from top to bottom are signals for 4–8 kHz, 2–4 kHz, 1–2 kHz, and 0.5–1 kHz. ELF/VLF signals for the top three frequency bands remained at background levels, while a clear rise can be seen in the lowest band (0.5–1 kHz) between ∼1440 and ∼1620 UT. Figure 4b is the temporal profile of the 0.5–1 kHz band signals observed at the AP1 station. Signals detected between ∼1530 and ∼1630 UT are at background levels. No ELF/VLF were observed at this station, which is likely to be located on open field lines at latitudes well poleward of the chorus source region. Figure 4c presents frequency-time spectrograms obtained at AP2 and SPA at 1505:30, 1605:30, and 1635:30 UT. Discrete elements can be seen in AP2 data at ∼0.5 kHz at 1605:30 UT, but overall the emissions are rather structureless. The intensified ∼0.5 kHz waves are responsible for the

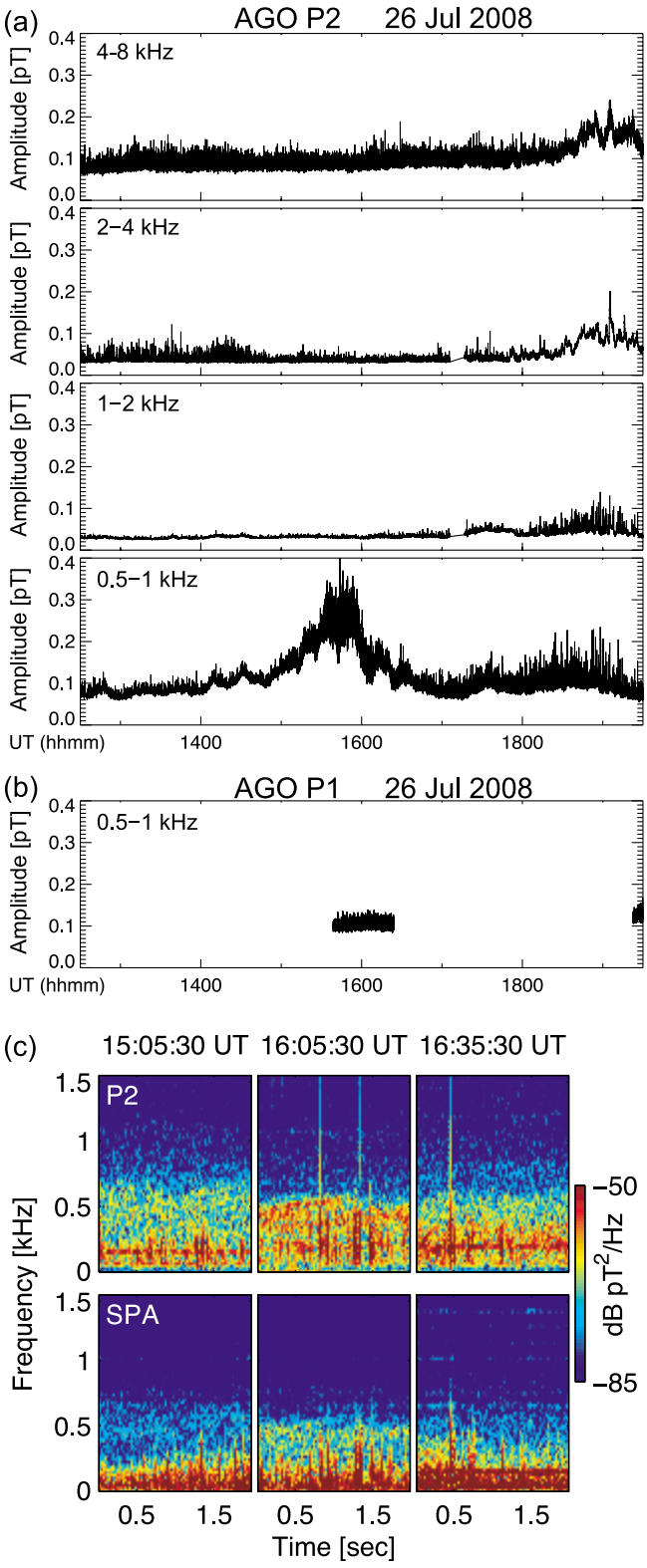

Figure 4. (a) ELF/VLF signals detected at the AP2 station between 1230 and 1930 UT for 4–8 kHz, 2–4 kHz, 1–2 kHz, and 0.5–1 kHz bands from top to bottom. (b) 0.5–1 kHz signals detected at the AP1 station. (c) Power spectrograms of ELF/VLF waves captured at (top) AP2 and (bottom) SPA at 15:05:30 UT, 16:05:30 UT, and 16:35:30 UT from left to right.

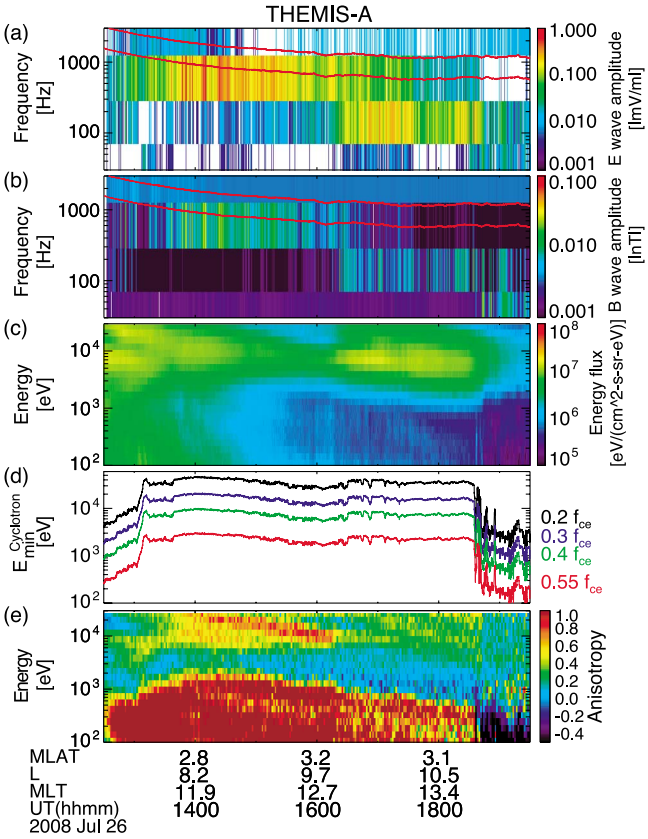

Figure 5. Spectrograms of (a) electric field and (b) magnetic field wave power obtained from the filter bank data of the EFI and SCM instruments onboard THEMIS A. Thin and thick red lines drawn on the spectrograms represent f_{ce} and 0.5 f_{ce}, where f_{ce} is the local electron cyclotron frequency calculated from the magnetic field data from the FGM instrument. (c) Energy-time diagram of the omnidirectional electron energy flux observed by THEMIS A and (d) the minimum electron energy for cyclotron resonance with chorus waves with frequencies of 0.2 f_{ce} (black), 0.3 f_{ce} (blue), 0.4 f_{ce} (green), and 0.55 f_{ce} (red) and (e) anisotropy factor of electrons estimated from THEMIS-A observations.

wave power increase in the 0.5–1 kHz band. Data from SPA show extremely weak signatures of chorus at 16:05:30 UT.

[27] Since the wave power at higher frequencies at AP2 is very low, we can be confident that the rise in the lowest band is not due to auroral hiss, which usually causes high wave power at high frequencies with decreasing amplitude in the lower frequency channels, or due to wind noise, which can essentially cause the ELF/VLF receiver antennas to oscillate and accordingly rise/fall signals in all the channels. A wave frequency of 0.5 kHz at high-latitude PENGUIn/AGO stations is typically in the frequency range of lower-band chorus waves generated inside the FOV of the stations, that is, in the outer magnetosphere. We will confirm this by comparing with conjugate observations made by THEMIS in the next section.

3.3. THEMIS Observations

[28] Figure 5a shows electric field wave amplitude from the filter bank data recorded by EFI onboard THEMIS-A. Figure 5b plots magnetic field wave amplitude from the filter bank data recorded by SCM onboard THEMIS-A. In both fields, the amplitude of the 287–1240 Hz band was enhanced between ~1330 and ~1630 UT. The 72.2–287 Hz band intensified intermittently after 1600 UT. The two solid red lines in each panel represent the local electron cyclotron frequency (f_{ce}) and 0.5 f_{ce}.

[29] Figure 5c is an energy-time plot of the omnidirectional flux of electrons observed by ESA onboard THEMIS-A, and shows no clear energy-dispersed injections at >1 keV which are associated with substorm activity.

[30] Figure 5d is the minimum resonant energy of first-order electron cyclotron resonance for wave frequencies of 0.2, 0.3, 0.4, and 0.55 f_{ce} [*Kennel and Petschek*, 1966], which is defined as

$$E_{\min} = \frac{m_e c^2}{2} \frac{\Omega_e^2}{\omega_{pe}^2} \frac{\Omega_e}{\omega} \left(1 - \frac{\omega}{\Omega_e}\right)^3,$$

where m_e is the electron mass, $\Omega_e = 2\pi f_{ce}$, ω_{pe} is the plasma angular frequency, and ω is the wave angular frequency ($=2\pi f$). The minimum resonant energies of lower-band dayside chorus are mostly covered well by the ESA energy range. Figure 5e shows an energy spectrogram of the electron anisotropy factor calculated for a fixed electron kinetic energy (mean value in the specified energy range) from the observed pitch angle distributions [*Chen et al.*, 1999; *Li et al.*, 2010]. The anisotropy factor is defined as

$$A = \frac{\int_0^{\pi/2} f(E,\alpha_0) \sin^3\alpha_0 d\alpha_0}{2\int_0^{\pi/2} f(E,\alpha_0) \cos^2\alpha_0 \sin\alpha_0 d\alpha_0} - 1,$$

where α_0 is the equatorial pitch angle, E is the kinetic energy, and f is the electron phase space density. The value of A around the minimum resonant energy (10–40 keV) was between 0.5 and 1.0 during the intensification of the 287–1240 Hz band wave (~1330–~1630 UT) shown in the filter bank data (Figures 5a and 5b), indicating that electron pitch angle distributions were pancake-like.

[31] High-resolution wave burst data were recorded by THEMIS-A located at (L, MLAT, MLT) = (8.5, 2.8°, 12.1 h) at 1422 UT, around the peak of the 287–1240 Hz band intensification. Figures 6a–6c plot three components of Poynting flux in the field-aligned coordinate with radially outward (Pr), eastward (Pe), and upward (Pup); the negative Pup represents northward, that is, away from the equator in this case. Figure 6d is the magnetic wave amplitude for the lower-band (blue) and upper-band chorus (red) waves. Figures 6e and 6f show spectrograms of the frequency-time spectrogram in electric and magnetic fields, respectively. The spectrograms show clear rising tone elements at 500–700 Hz (~0.35–~0.45 f_{ce}). Wave polarization properties were calculated from three magnetic components of waveform data following the method by *Bortnik et al.* [2007a] (an implementation of *Means* [1972]). Figures 6g–6i are the wave normal angle, ellipticity, and polarization ratio. The polarization ratio represents the ratio of polarized power to total power. The ellipticity is defined in this study as the ratio of the minor axis to the major axis in the plane perpendicular to the wave vector with a positive (negative)

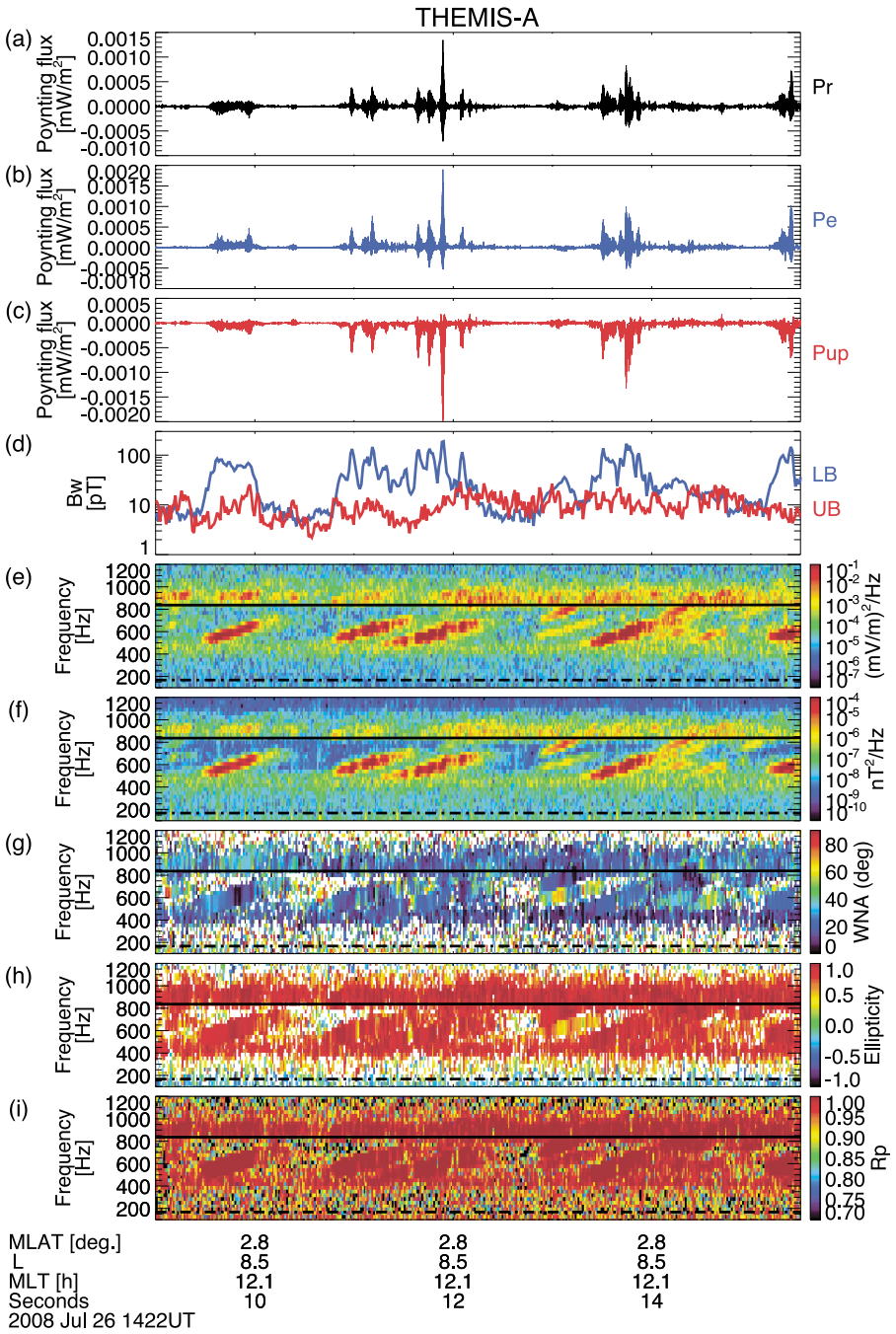

Figure 6. High-resolution wave burst data from THEMIS A. (a–c) Three components of Poynting flux in the field-aligned coordinate. Negative Pup represents the direction away from the equator. (d) Magnetic wave amplitude for the lower-band (blue) and upper-band chorus (red). (e) Frequency-time spectrogram of electric and (f) magnetic field waves. (g) Wave normal angle, (h) ellipticity, and (i) polarization ratio. The black solid and dashed lines in Figures 6e–6i represent 0.5 f_{ce} and 0.1 f_{ce}, respectively.

value corresponding to right-hand (left-hand) rotation about the wave vector.

[32] In Figures 6e–6i, the black solid line and dash-dotted line represent 0.5 f_{ce} and 0.1 f_{ce}. It is evident that the wave polarization is right-hand circular and the waves are propagating at small (<20°) to the ambient magnetic field. These properties are also consistent with chorus waves.

[33] Wave features presented in Figure 6 confirm that THEMIS A did capture lower-band chorus waves with rising tone elements that were propagating quasi-parallel to the ambient magnetic field, away from the equator. The peak frequency of the chorus waves is 500–600 Hz, which is consistent with the frequency of structureless ELF/VLF elements detected at the AP2 station (Figure 4b). We therefore conclude that ELF/VLF waves seen at AP2 most likely originated from the lower-band chorus waves observed by THEMIS.

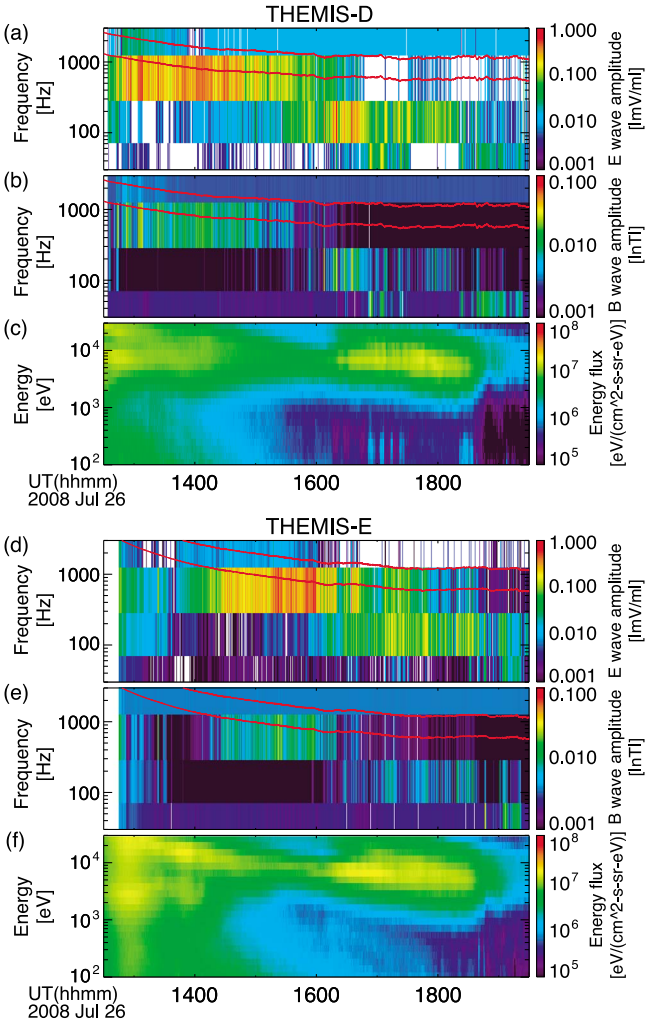

Figure 7. Spectrograms of (a and d) electric field and (b and e) magnetic field wave power obtained from the filter bank data of the EFI and SCM instruments and (c and f) energy-time diagram of the omnidirectional electron energy flux. Figures 7a–7c and 7d–7f show observations by THEMIS D and THEMIS E, respectively.

[34] Figure 7 presents the filter bank data and electron energy-time diagram for THEMIS D and E in the same format as Figures 5a–5c. THEMIS D was located at (L, MLAT, MLT) = (8.64, 4.75, 12.0 h) and THEMIS E was at (L, MLAT, MLT) = (6.91, 6.83, 11.2 h) at 1400 UT. No high-resolution wave burst data are available from these two probes for the interval of interest. The 287–1240 Hz band wave amplitude has a similar temporal profile to that observed by THEMIS-A (Figures 5a and 5b), with wave intensification at THEMIS E occurring ~1.5 h later than THEMIS A and D. The time delay is a spatial effect, as discussed in the next section. No clear energy-dispersed electron injections were observed by either probe during the time of interest.

4. Wave Spatial Distributions and Magnetic Field Configuration

[35] As mentioned in Section 3.1 and shown in Figures 2 and 3, the solar wind dynamic pressure was almost constant and geomagnetic conditions were quiet on 26 July 2008, especially during and surrounding the hours of the chorus events under study. The THEMIS spacecraft on the dayside did not see energy-dispersed electron injections when they registered the intensification of chorus waves. The observations suggest that the observed chorus waves were not generated as a result of concurrent/earlier substorm activity or sudden compression of the dayside magnetosphere. We therefore conclude that the wave amplitude variations observed by three THEMIS spacecraft (Figures 5 and 7) likely represent not temporal but rather spatial variations of chorus wave power.

4.1. Spatial Distributions of Dayside Chorus

[36] Figures 8a and 8b are the spatial distribution of the wave electric and magnetic field amplitudes, respectively. We used the wave amplitude of the 287–1240 Hz band from filter bank data recorded by EFI and SCM (Figures 5 and 7) as the band covers wave frequencies simultaneously observed at AP2 in Antarctica. The THEMIS positions were mapped onto the X-Y plane in SM coordinates along the TS01 model field lines. Color represents the wave amplitude in the same scale as in Figures 5 and 7. The colored line denoted AP2 is the trajectory of the AP2 location mapped onto the SM-coordinate X-Y plane along the TS01 model field lines; color represents the amplitude of the 0.5–1 kHz wave band (Figure 4a, bottom).

[37] The spatial distribution is quite consistent between the THEMIS observations and the ground-based observations in Antarctica. The chorus wave intensification was localized in narrow ranges of MLT (12.5 < MLT < 13.5 h) and radial distance ($7 < R < 10$ R_E, where R is the radial distance when mapped onto the SM-coordinate X-Y plane). In addition, the THEMIS multispacecraft observations yield the conclusion that the localized chorus intensification persisted for at least 1.5 h in the same location. THEMIS E trailed THEMIS D along almost the same trajectory with the spacecraft separation about 1.5 h. Both spacecraft observed a similar time profile of 287–1240 Hz wave intensification, as shown in Figure 7.

4.2. Magnetic Field Configuration During Chorus Intensification

[38] In order to study the configuration of the dayside magnetosphere during the period of chorus intensification, we examined how the magnetic field strength changes along a field line on which a THEMIS spacecraft was located. Figure 9 shows the variations of the magnetic field strength as a function of magnetic latitude for a set of field lines that THEMIS probes crossed during their outbound paths. Each panel contains a large number of colored curved lines. A curved line corresponds to the latitudinal profile of the magnetic field strength for a field line where a THEMIS spacecraft was located at a specific time; color code represents the magnetic/electric field wave amplitude from THEMIS filter bank data (Figures 5 and 7). We derived the field lines and field strength from the TS01 model.

[39] During the periods of chorus wave intensification, as colored in orange to red, the magnetic field configuration is less dipole-like, affected by solar wind compression, with the field-aligned gradient of the magnetic field strength (dB/ds) nearly zero over a long distance along the field line

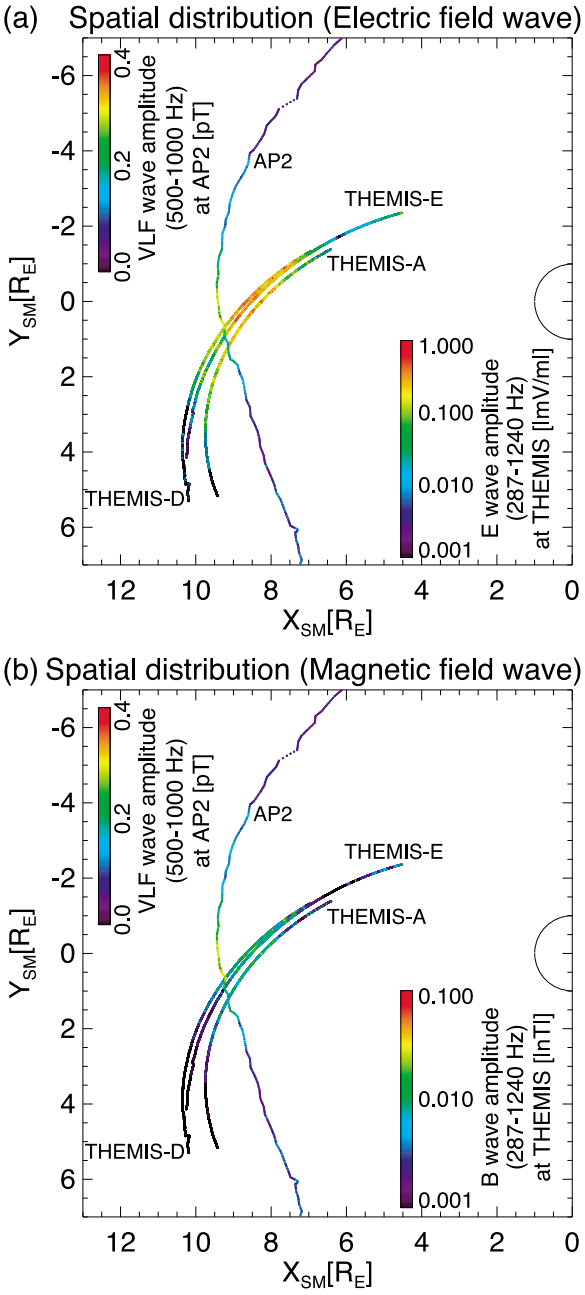

Figure 8. Spatial distributions on the X-Y plane in SM coordinates of (a) electric and (b) magnetic field wave amplitude from THEMIS filter bank data along with those of ELF/VLF wave amplitude observed at AP2. THEMIS positions and AP2 locations are mapped onto the X-Y plane along field lines derived from the TS01 model. Color on the trajectories represents wave amplitudes, as indicated at the right bottom for THEMIS observations and left top for the ground-based observations. The color scale for the THEMIS observations is the same as in Figures 5 and 7.

($\sim -20° <$ MLAT $< 20°$). When THEMIS occupied more dipole-like field lines, on the other hand, chorus waves were not enhanced. As THEMIS moved into the region where magnetic field lines have two minima off the magnetic equator (i.e., off-equatorial minimum-*B* pockets), the chorus wave amplitude decreased. These characteristics of the occurrence of chorus wave intensification are confirmed by both electric and magnetic field wave data from all three THEMIS spacecraft.

[40] To examine if the dayside magnetic field configuration is well reproduced by the TS01 model for the interval shown in this study, we compared the TS01 magnetic field with the THEMIS observations of the magnetic field. Figure 10a shows the magnetic field observed by THEMIS A (black) and derived from the TS01 model (blue) between 1230 and 1930 UT, and Figure 10b is the difference between the TS01 model and observations made by three THEMIS observations. The time period of the chorus amplification observed by THEMIS is highlighted in orange. The deviation from the TS01 model is within 5 nT in magnitude, 10° in the angle from the magnetic equator, 10° in the MLT direction. The deviation in the MLT direction decreases down to $\sim -30°$ at $\sim$1820 UT because the TS01 model field changed by $\sim$20°, while the other two components do not show significant changes. The variation is likely due to a sudden change in the IMF direction as observed by THEMIS B (shown in Figure 3).

[41] Figure 11 presents the latitudinal profile of the magnetic field strength for a set of field lines to which the AP2 station is connected based on the TS01 model. Color represents power of 500–1000 Hz ELF/VLF waves. Again, the wave power is increased when field lines have nearly zero *dB/ds* over a wide range of MLAT.

5. Summary and Discussions

[42] We examined ELF/VLF waves simultaneously observed at PENGUIn/AGO stations in Antarctica and by three THEMIS probes under quiet solar wind and geomagnetic conditions on 26 July 2008. Observations are summarized as follows.

[43] 1. Solar wind dynamic pressure observed by THEMIS B at $X_{GSE} \sim 28\ R_E$ was $\sim$0.8 nPa and almost constant. IMF at THEMIS was not fluctuating and its Z component was ~ -2 nT.

[44] 2. At the AP2 station, an enhancement of ELF/VLF signals was observed at the 0.5–1 kHz band with the peak at $\sim$1540 UT and $\sim$1210 MLT. ELF/VLF signals at higher frequency bands (1–2 kHz, 2–4 kHz, and 4–8 kHz) did not increase. Structureless and discrete elements were seen at $\sim$0.5 kHz.

[45] 3. THEMIS A, D, and E traveled in their outbound paths in the outer magnetosphere around noon. The foot points passed through the field-of-view (FOV) of the ELF/VLF receiver at AGO P2 between $\sim$15 and $\sim$17 UT.

[46] 4. THEMIS A registered lower-band chorus waves with rising tones elements at the frequency of 500–700 Hz (0.3–0.4 f_{ce}) at $\sim$1422 UT and $\sim$1200 MLT near the magnetic equator (MLAT $\sim$ 3°) at the radial distance of $\sim 8\ R_E$. The Poynting vector indicates that the chorus waves were propagating away from the equator. The wave normal angle is estimated to be smaller than $\sim$20°.

[47] 5. The electric and magnetic field wave amplitudes at THEMIS A were enhanced at the 287–1240 Hz band between $\sim$1330 and $\sim$1700 UT, when THEMIS A traveled in the outer magnetosphere around noon. THEMIS A electron data indicate no dispersed electron injections during the wave enhancement. The anisotropy factor *A* of electrons

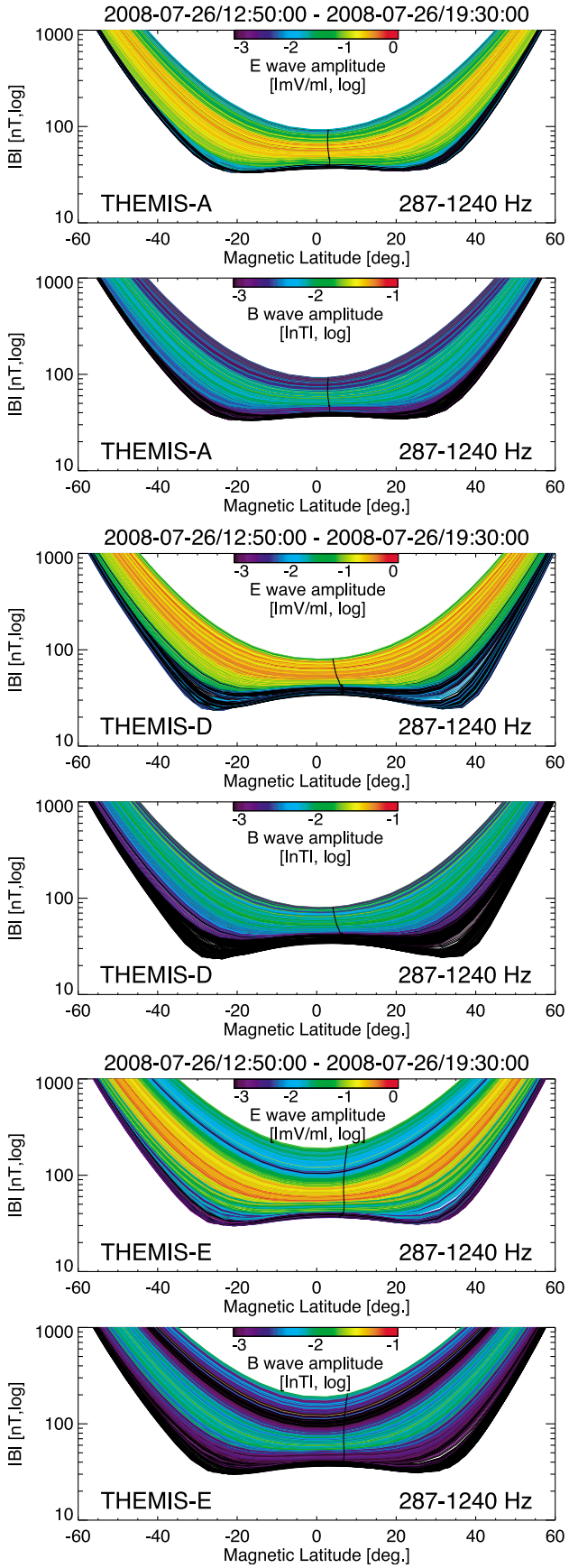

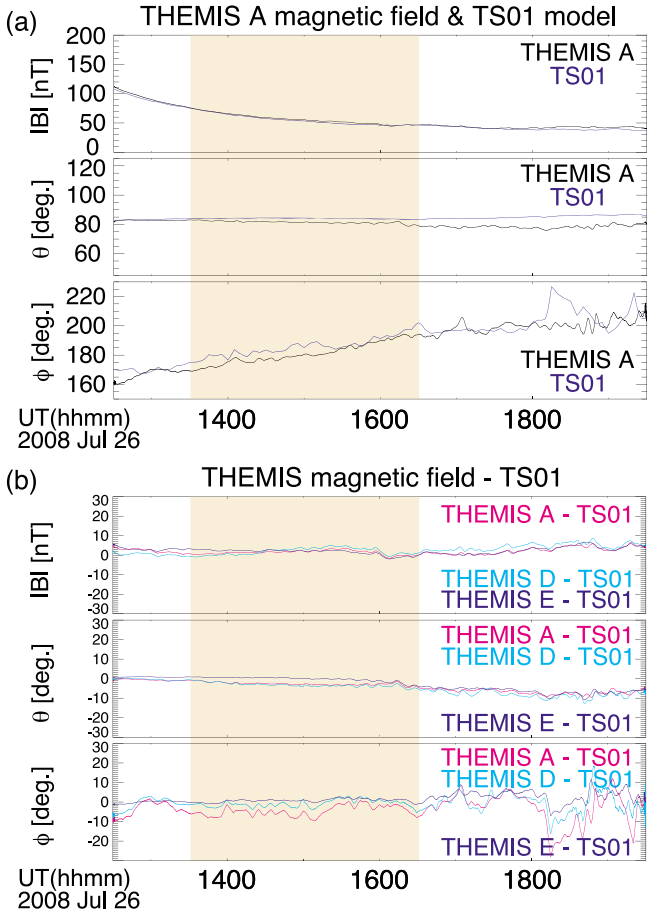

Figure 10. (a) Magnetic field observed by THEMIS A (black) and derived from the TS01 model (blue) between 1230 and 1930 UT; from top to bottom, the magnitude, the angle from the magnetic equatorial plane, and the angle from the X direction in SM coordinates. The time period of the chorus wave amplification observed by THEMIS (i.e., 1330–1630 UT) is highlighted in orange. (b) Differences in the magnetic field between from the TS01 model and from the THEMIS A (magenta), D (cyan), and E (blue) observations in the same format as Figure 10a.

with energies of 10–25 keV was ~1 at maximum. The minimum resonant energy was estimated to be ~10 keV for 0.4 f_{ce} waves and ~20 keV for 0.3 f_{ce} waves.

[48] 6. THEMIS D and E observed electric and magnetic field wave intensification at the 287–1240 Hz band. The

Figure 9. Variations of the magnetic field strength as a function of magnetic latitude. Each panel shows superposition of a large number of colored curves, each of which corresponds to the latitudinal variations of a field line on which a THEMIS spacecraft is located at a given time. The curves are color-coded by the 287–1240 Hz wave amplitude from the THEMIS filter bank data, as indicated at the middle top. The color scale is the same as shown in Figures 5, 7, and 8. The thick black lines overplotted on the colored curves represent the trajectories of the THEMIS spacecraft on the B vs MLAT plots. Field lines and their field-aligned variations of the field strength are derived from the TS01 model.

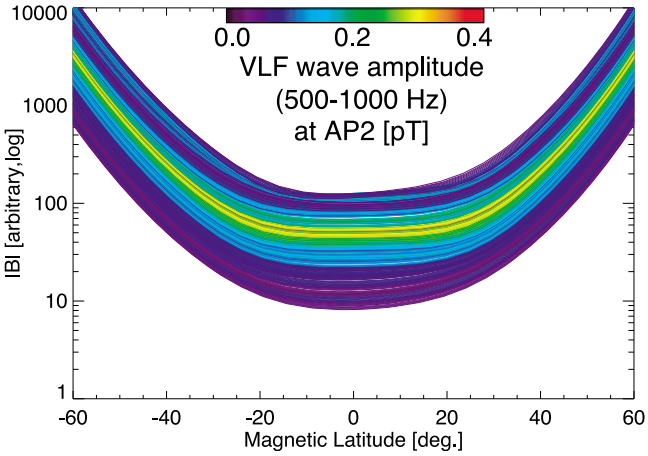

Figure 11. Variations of the magnetic field strength as a function of magnetic latitude: each curve corresponds to the latitudinal variations of a field line connected to the AP2 station at a given time. The curves are color-coded by the 500–1000 Hz ELF/VLF wave amplitude detected at AP2 as shown in Figure 4a (bottom). Field lines and their field-aligned variations of the field strength are derived from the TS01 model.

time profile of the wave intensification is similar to that observed by THEMIS A. Electron data indicate no energy-dispersed electron injections during the wave intensification.

[49] 7. The wave enhancements were spatially localized in the outer magnetosphere ($7 < R < 10$ R_E) around noon ($12.5 <$ MLT < 13.5 h). The localized enhancements persisted for at least 1.5 h in the same location. The ELF/VLF signal variations observed at AP2 are quite consistent with the global distribution of the wave enhancements.

[50] 8. The long-lasting and localized wave intensification occurred on field lines that exhibit nearly zero $dB/ds \sim 0$ in a wide range of MLAT ($\sim$20 deg.). A similar feature was found for the enhancements of ELF/VLF signals at AP2, where FOV scanned the entire dayside outer magnetosphere as the Earth rotated.

[51] The time profile of ELF/VLF signals at AP2 and the snapshots of ELF/VLF power spectrograms are consistent with the THEMIS observations. During conjugate observations at $\sim$16 UT, 0.5 f_{ce} at THEMIS was $\sim$700Hz and the chorus intensification occurred at between 0.3 and 0.4 f_{ce}, equivalent to $\sim$0.5 kHz, which is the same frequency as the discrete elements observed at AP2. We therefore conclude that ELF/VLF waves seen at AP2 were most likely the same lower-band chorus waves observed on THEMIS.

5.1. Long-Lasting Chorus in the Dayside Uniform Zone (DUZ)

[52] The most notable feature of the observed chorus waves is that the wave amplification persisted for >1.5 h in the same location, implying that the persistency was not due to drift of energetic electrons of plasma sheet origin or corotation of enhanced/depleted cold plasma population. The wave amplification occurred within a specific magnetic field configuration, namely on field lines that exhibit nearly zero *dB/ds* over a wide range of magnetic latitude. Smaller *dB/ds* favors the phase-trapping of electrons in the potential well of the wave, which is considered a necessary condition for nonlinear wave growth [*Nunn*, 1974; *Dowden et al.*, 1978; *Bell and Inan*, 1981; *Omura et al.*, 1991]. *Omura et al.* [2008] showed that the chorus wave amplitude is sustained by the increasing inhomogeneity of the dipole field. Our results confirm that such a flattened field configuration (i.e., nearly zero *dB*/*ds* in a long distance along *B*) is particularly favorable for chorus wave generation, as *Spasojević and Inan* [2010] asserted. The wave amplification occurred adjacent to, but not exactly at the L-shell corresponding to the off-equatorial minimum-*B* pockets. We thus conclude that the observed long-lasting, localized, quiet time dayside chorus amplification was due to the nearly zero *dB*/*ds* conditions that occur naturally in the dayside uniform zone (DUZ), the transition region between the near-Earth dipole zone and the compressed, off-equatorial double-minimum field configuration closer to the magnetopause (called the dayside outer zone (DOZ) [*Tsurutani et al.*, 2009]). Figure 12 illustrates the DUZ, DOZ, and the dayside dipolar zone (DDZ) in the X-Z plane and the field-aligned profile of the magnetic field strength for the three regions.

5.2. Generation of Rising Tone Elements

[53] The chorus waves observed by THEMIS A at $\sim$3° MLAT consisted of rising tone elements and were propagating away from the magnetic equator. As indicated by an anisotropic factor calculated from THEMIS electron observations, electron velocity distributions were pancake-like. We conclude that the chorus rising tone elements were generated at the magnetic equator through the nonlinear growth following the linear growth. *Omura et al.* [2008] concluded that the seed waves that trigger rising tone chorus elements are generated near the magnetic equator, where the temporal frequency variation or the second-order phase variation in time, maximizes the nonlinear growth rate.

5.3. Source of Free Energy

[54] The observations indicate >1.5 h persistence of localized chorus wave generation in a steady state magnetosphere under quiet geomagnetic conditions. To account for the excitation of chorus, the linear growth requires high fluxes of resonant electrons (typically with energies of 1–100 keV), sufficient anisotropy at resonant energies, and small ratio of plasma frequency to cyclotron frequency. It is a reasonable interpretation that the free energy was not brought in by electrons freshly and strongly injected from the plasma sheet during a course of substorms, because THEMIS did not observe dispersed injections and no clear substorm activity was confirmed during the examined interval. The differential energy flux of $\sim$10 keV electrons was $\sim 10^7$ [eV/(cm^2 s sr eV)] during the wave excitation, which is smaller than that after substorm-associated injections. We suggest that the free energy source is anisotropy that develops in the electron population that was continuously supplied to the inner magnetosphere under conditions of small but continuous southward IMF or was injected many hours before the wave excitation and trapped in a steady state magnetosphere. The IMF Z-component was in fact slightly negative right upstream of the bow shock during chorus intensification. The solar wind dynamic pressure was almost constant for a period of >5 h that covers the chorus

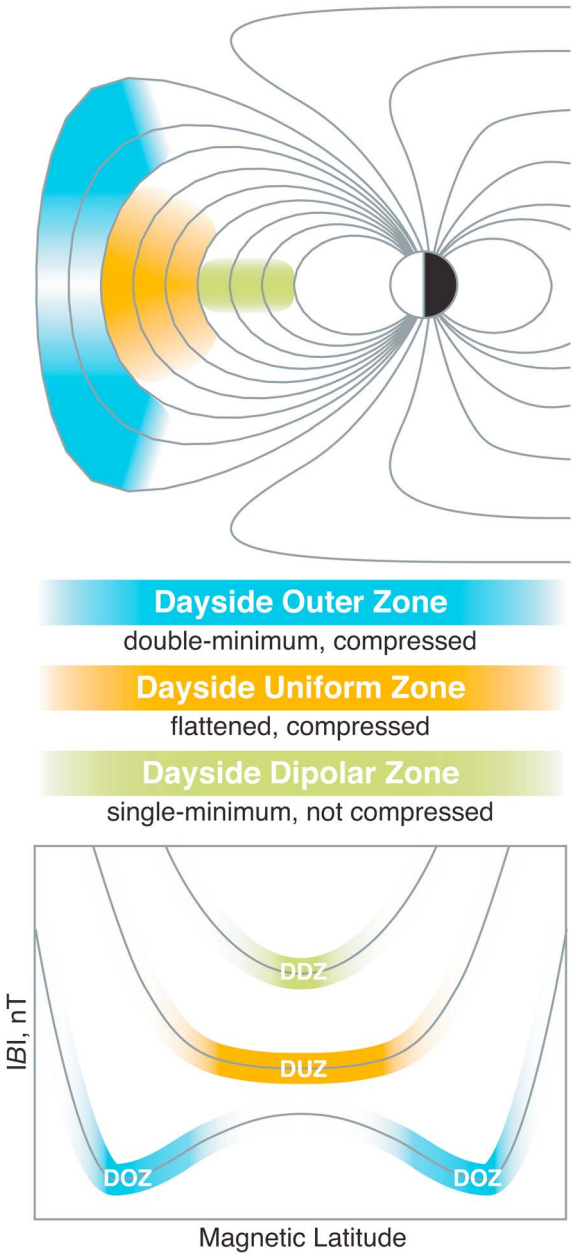

Figure 12. Schematic diagrams of the dayside uniform zone (DUZ), the transition region between the near-Earth dipole (dayside dipolar zone, DDZ) and the compressed, off-equatorial double-minimum field configuration closer to the magnetopause (dayside outer zone, DOZ, proposed by *Tsurutani et al.* [2009]), illustrating (top) the regions in the X-Z plane and (bottom) the field-aligned profile of the magnetic field strength for the regions. Field lines in the DUZ exhibit nearly zero field-aligned *B* gradient over a wider range of magnetic latitudes than in the DDZ and DOZ. The long-lasting, localized, quiet time dayside chorus examined in this study was generated in the DUZ but not in the DDZ or DOZ.

wave excitation, likely leading to a steady state magnetosphere that allows energetic electrons to be trapped for a long time. The development of electron anisotropy may be due to electron scattering through interactions with magnetospheric waves or/and electron drift shell splitting which causes a larger number of equatorially mirroring electrons to reach the outer magnetosphere than electrons mirroring at high latitudes.

5.4. Effects of Minimum-*B* Pockets on Chorus Generation

[55] Chorus waves with frequencies of 500–700 Hz were not observed when THEMIS crossed field lines that display minimum-*B* pockets at high latitudes. However, the possibility of dayside chorus generation near the minimum-*B* pockets cannot be completely ruled out. Low frequency electric and magnetic field waves (~200 Hz) were found in the fast-survey data from THEMIS A at 1830 UT (not shown here). According to the Tsyganenko field model, THEMIS A was located on field lines with off-equatorial double-minimum *B*. The observed wave frequency was between 0.1 and 0.2 f_{ce}, where f_{ce} is calculated based on the magnetic field strength close to the magnetic equator (observed by THEMIS). The normalized frequency may be a little higher (by a factor of 2 to 3) if we use the *B* strength of the local minima. These lower-frequency waves may have been generated at/close to the local minimum/minima, as a scenario of DOZ chorus proposed by *Tsurutani and Smith* [1977].

5.5. ULF or Density Modulation

[56] *Li et al.* [2011b, 2011c] reported dawnside chorus wave events that indicate a good correlation with magnetic field oscillations with a period of ULF waves. They also showed that some chorus intensifications are well associated with density enhancements/depletions, although the underlying physical processes controlling these oscillations are still under investigation [*Bell et al.*, 2009; *Haque et al.*, 2011]. The DUZ chorus event examined in this study, on the other hand, does not show clear ULF waves or density variations during the chorus wave intensification. This is consistent with the results of the spatial distribution of ULF modulation events, which preferentially occur on the dawnside [*Li et al.*, 2011c].

5.6. Possible Contribution of DUZ Chorus to Radiation Belt Dynamics

[57] Whistler mode chorus waves play an important role in the dynamics of radiation belt electrons [e.g., *Friedel et al.*, 2002; *Miyoshi et al.*, 2003; *Li et al.*, 2007; *Shprits et al.*, 2007; *Summers et al.*, 2007; *Bortnik et al.*, 2007b]. Chorus waves can experience gyroresonant interactions with mid-energy (~1–100 keV) electrons, providing a mechanism for local acceleration of those electrons to relativistic energies (>1 MeV). Chorus waves can also resonate with relativistic electrons near the loss cone, contributing to pitch angle scattering and loss of the relativistic electrons into the atmosphere. The scattering of energetic electrons by discrete chorus elements can result in <1 s intensifications of precipitation known as microbursts [e.g., *Lorentzen et al.*, 2001; *Millan and Thorne*, 2007]. We speculate that the DUZ chorus makes a significant contribution to radiation belt dynamics, particularly under quiet geomagnetic conditions.

The DUZ should exist anytime in the Earth's dayside magnetosphere and may facilitate chorus amplification even under conditions of low source electron flux, as shown in the present study. It may also be important to understand the extent of the steady dayside magnetosphere compression, since this determines the size of the DUZ.

6. Conclusions

[58] We examined simultaneous observations of ELF/VLF waves detected around noon by three THEMIS spacecraft in the outer magnetosphere and at PENGUIn/AGO stations in Antarctica at high geomagnetic latitudes. The waves were excited during a period of steady solar wind with correspondingly quiet geomagnetic conditions, with no substorm activity. The conjugate observation confirmed that the observed waves were whistler mode chorus waves with rising-tone elements. The waves persisted for at least 1.5 h in the same location, in a narrow range of MLT and radial distance, that did not seem to corotate with the Earth or drift with the energetic electrons. The waves were excited on field lines that exhibit nearly zero field-aligned B gradient over a wide range of magnetic latitudes. The waves propagated away from the equator, quasi-parallel to the ambient magnetic field, indicating generation at the magnetic equator. We conclude that the long-lasting, localized, quiet time dayside chorus amplification was due to the nearly zero dB/ds conditions. The magnetic field configuration occurs naturally in the dayside uniform zone (DUZ), the transition region between the near-Earth dipole and the compressed, off-equatorial double-minimum field configuration found closer to the magnetopause. The free energy for the wave growth of the quiet-time DUZ chorus may have resulted from anisotropy that develops in the electron population that was continuously supplied to the inner magnetosphere under conditions of small but continuous southward IMF or was injected many hours before the wave excitation and were trapped in a steady state magnetosphere. The development of electron anisotropy may be due to electron scattering through interactions with magnetospheric waves or/and drift shell splitting which causes a larger number of equatorially mirroring electrons to reach the outer magnetosphere than electrons mirroring at high latitudes.

[59] **Acknowledgments.** We are grateful to L. J. Lanzerotti and A. J. Gerrard for their helpful comments. We acknowledge NASA contract NAS5-02099 for use of data from the THEMIS mission; specifically, J. W. Bonnell and F. S. Mozer for use of EFI data, C. W. Carlson and J. P. McFadden for use of ESA data, A. Roux and O. LeContel for use of SCM data, K. H. Glassmeier, U. Auster, and W. Baumjohann for the use of FGM data provided under the lead of the Technical University of Braunschweig and with financial support through the German Ministry for Economy and Technology and the German Center for Aviation and Space (DLR) under contract 50 OC 0302. Wind and GOES data are available through Coordinated Data Analysis Web (CDAWeb), NASA. The SYM-H and provisional AE indices were provided by Data Analysis Center for Geomagnetism and Space Magnetism in Kyoto, Japan. This work was supported by NASA grant NAS5-01072 to New Jersey Institute of Technology. The work at Stanford University was supported by the National Science Foundation under grant 0840058. J. Bortnik and W. Li gratefully acknowledge the support of NASA through grant NNX11AD75G. This work was carried out by the joint research program of the Solar-Terrestrial Environment Laboratory, Nagoya University. Figure 12 was drawn by Mayuko Keika.

[60] Robert Lysak thanks the reviewers for their assistance in evaluating this paper.

References

Abel, G. A., M. P. Freeman, A. J. Smith, and G. D. Reeves (2006), Association of substorm chorus events with drift echoes, *J. Geophys. Res.*, *111*, A11220, doi:10.1029/2006JA011860.

Angelopoulos, V. (2008), The THEMIS mission, *Space Sci. Rev.*, *141*, 5–34, doi:10.1007/s11214-008-9336-1.

Auster, H. U., et al. (2008), The THEMIS Fluxgate Magnetometer, *Space Sci. Rev.*, *141*(1–4), 235–264, doi:10.1007/s11214-008-9365-9.

Bell, T. F., and U. S. Inan (1981), Transient nonlinear pitch angle scattering of energetic electrons by coherent VLF wave packets in the magnetosphere, *J. Geophys. Res.*, *86*(A11), 9047–9063, doi:10.1029/JA086iA11p09047.

Bell, T. F., U. S. Inan, N. Haque, and J. S. Pickett (2009), Source regions of banded chorus, *Geophys. Res. Lett.*, *36*, L11101, doi:10.1029/2009GL037629.

Bonnell, J., F. S. Mozer, G. T. Delory, A. J. Hull, R. E. Ergun, C. M. Cully, V. Angelopoulos, and P. R. Harvey (2008), The Electric Field Instrument (EFI) for THEMIS, *Space Sci. Rev.*, *141*(1–4), 303–341, doi:10.1007/s11214-008-9469-2.

Bortnik, J., J. W. Cutler, C. Dunson, and T. E. Bleier (2007a), An automatic wave detection algorithm applied to Pc1 pulsations, *J. Geophys. Res.*, *112*, A04204, doi:10.1029/2006JA011900.

Bortnik, J., R. M. Thorne, and N. P. Meredith (2007b), Modeling the propagation characteristics of chorus using CRRES suprathermal electron fluxes, *J. Geophys. Res.*, *112*, A08204, doi:10.1029/2006JA012237.

Bortnik, J., R. M. Thorne, and N. P. Meredith (2008), The unexpected origin of plasmaspheric hiss from discrete chorus emissions, *Nature*, *452*(7183), 62–66, doi:10.1038/nature06741.

Bunch, N. L., M. Spasojević, and Y. Y. Shprits (2011), On the latitudinal extent of chorus emissions as observed by the Polar Plasma Wave Instrument, *J. Geophys. Res.*, *116*, A04204, doi:10.1029/2010JA016181.

Bunch, N. L., M. Spasojevic, and Y. Y. Shprits (2012), Off-equatorial chorus occurrence and wave amplitude distributions as observed by the Polar Plasma Wave Instrument, *J. Geophys. Res.*, *117*, A04205, doi:10.1029/2011JA017228.

Burtis, W. J., and R. A. Helliwell (1969), Banded chorus: A new type of VLF radiation observed in the magnetosphere by OGO 1 and OGO 3, *J. Geophys. Res.*, *74*(11), 3002–3010, doi:10.1029/JA074i011p03002.

Burton, R. K., and R. E. Holzer (1974), The origin and propagation of chorus in the outer magnetosphere, *J. Geophys. Res.*, *79*(7), 1014–1023, doi:10.1029/JA079i007p01014.

Chen, M. W., J. L. Roeder, J. F. Fennell, L. R. Lyons, R. L. Lambour, and M. Schulz (1999), Proton ring current pitch angle distributions: Comparison of simulations with CRRES observations, *J. Geophys. Res.*, *104*(A8), 17,379–17,389, doi:10.1029/1999JA900142.

Cully, C. M., R. E. Ergun, K. Stevens, A. Nammari, and J. Westfall (2008), The THEMIS Digital Fields Board, *Space Sci. Rev.*, *141*(1–4), 343–355, doi:10.1007/s11214-008-9417-1.

Dowden, R. L., A. D. McKay, L. E. S. Amon, H. C. Koons, and M. H. Dazey (1978), Linear and nonlinear amplification in the magnetosphere during a 6.6-kHz transmission, *J. Geophys. Res.*, *83*(A1), 169–181, doi:10.1029/JA083iA01p00169.

Friedel, R. H. W., G. D. Reeve, and T. Obara (2002), Relativistic electron dynamics in the inner magnetosphere—A review, *J. Atmos. Sol. Terr. Phys.*, *64*(2), 265–282, doi:10.1016/S1364-6826(01)00088-8.

Fu, H. S., J. B. Cao, F. S. Mozer, H. Y. Lu, and B. Yang (2012), Chorus intensification in response to interplanetary shock, *J. Geophys. Res.*, *117*, A01203, doi:10.1029/2011JA016913.

Gail, W. B., and U. S. Inan (1990), Characteristics of wave-particle interactions during sudden commencements: 2. Spacecraft observations, *J. Geophys. Res.*, *95*(A1), 139–147, doi:10.1029/JA095iA01p00139.

Gail, W. B., U. S. Inan, R. A. Helliwell, D. L. Carpenter, S. Krishnaswamy, T. J. Rosenberg, and L. J. Lanzerotti (1990), Characteristics of wave-particle interactions during sudden commencements: 1. Ground-based observations, *J. Geophys. Res.*, *95*(A1), 119–137, doi:10.1029/JA095iA01p00119.

Haque, N., M. Spasojević, O. Santolík, and U. S. Inan (2010), Wave normal angles of magnetospheric chorus emissions observed on the Polar spacecraft, *J. Geophys. Res.*, *115*, A00F07, doi:10.1029/2009JA014717.

Haque, N., U. S. Inan, T. F. Bell, J. S. Pickett, J. G. Trotignon, and G. Facskó (2011), Cluster observations of whistler mode ducts and banded chorus, *Geophys. Res. Lett.*, *38*, L18107, doi:10.1029/2011GL049112.

Hayosh, M., O. Santolík, and M. Parrot (2010), Location and size of the global source region of whistler mode chorus, *J. Geophys. Res.*, *115*, A00F06, doi:10.1029/2009JA014950.

Horne, R. B., and R. M. Thorne (2000), Electron pitch angle diffusion by electrostatic electron cyclotron harmonic waves: The origin of pancake distributions, *J. Geophys. Res.*, *105*(A3), 5391–5402, doi:10.1029/1999JA900447.

Kasahara, Y., Y. Miyoshi, Y. Omura, O. P. Verkhoglyadova, I. Nagano, I. Kimura, and B. T. Tsurutani (2009), Simultaneous satellite observations of VLF chorus, hot and relativistic electrons in a magnetic storm "recovery" phase, *Geophys. Res. Lett.*, *36*, L01106, doi:10.1029/2008GL036454.

Kennel, C. F., and H. E. Petschek (1966), Limit on stably trapped particle fluxes, *J. Geophys. Res.*, *71*(1), 1–28, doi:10.1029/JZ071i001p00001.

Kim, K. C., D. Y. Lee, H. J. Kim, L. R. Lyons, E. S. Lee, M. K. Öztürk, and C. R. Choi (2008), Numerical calculations of relativistic electron drift loss effect, *J. Geophys. Res.*, *113*, A09212, doi:10.1029/2007JA013011.

Kimura, I. (1974), Interrelation between VLF and ULF emissions, *Space Sci. Rev.*, *16*, 389–411, doi:10.1007/BF00171565.

Kleimenova, N. G., O. V. Kozyreva, J. Manninen, and A. Ranta (2005), Unusual strong quasi-monochromatic ground Pc5 geomagnetic pulsations in the recovery phase of November 2003 superstorm, *Ann. Geophys.*, *23*, 2621–2634, doi:10.5194/angeo-23-2621-2005.

Kokubun, S., M. G. Kivelson, R. L. McPherron, C. T. Russell, and H. I. West (1977), OGO 5 observations of Pc 5 waves: Particle flux modulations, *J. Geophys. Res.*, *82*, 2774–2786, doi:10.1029/JA082i019p02774.

Kremser, G., A. Korth, J. A. Fejer, B. Wilken, V. A. Gurevich, and E. Amata (1981), Observations of quasi-periodic flux variations of energetic ions and electrons associated with Pc 5 geomagnetic pulsations, *J. Geophys. Res.*, *86*(A5), 3345–3356, doi:10.1029/JA086iA05p03345.

Le Contel, O., et al. (2008), First results of the THEMIS search coil magnetometers, *Space Sci. Rev.*, *141*(1–4), 509–534, doi:10.1007/s11214-008-9371-y.

LeDocq, M. J., D. A. Gurnett, and B. Hospodarsky (1998), Chorus source locations from VLF Poynting flux measurements with the Polar spacecraft, *Geophys. Res. Lett.*, *25*(21), 4063–4066, doi:10.1029/1998GL900071.

Lessard, M. R., et al. (2009), PENGUIn multi-instrument observations of dayside high-latitude injections during the 23 March 2007 substorm, *J. Geophys. Res.*, *114*, A00C11, doi:10.1029/2008JA013507. [Printed *115*(A1), 2010.]

Li, W., Y. Y. Shprits, and R. M. Thorne (2007), Dynamic evolution of energetic outer zone electrons due to wave-particle interactions during storms, *J. Geophys. Res.*, *112*, A10220, doi:10.1029/2007JA012368.

Li, W., R. M. Thorne, V. Angelopoulos, J. W. Bonnell, J. P. McFadden, C. W. Carlson, O. LeContel, A. Roux, K. H. Glassmeier, and H. U. Auster (2009), Evaluation of whistler-mode chorus intensification on the nightside during an injection event observed on the THEMIS spacecraft, *J. Geophys. Res.*, *114*, A00C14, doi:10.1029/2008JA013554. [Printed *115*(A1), 2010.]

Li, W., et al. (2010), THEMIS analysis of observed equatorial electron distributions responsible for the chorus excitation, *J. Geophys. Res.*, *115*, A00F11, doi:10.1029/2009JA014845.

Li, W., J. Bortnik, R. M. Thorne, and V. Angelopoulos (2011a), Global distribution of wave amplitudes and wave normal angles of chorus waves using THEMIS wave observations, *J. Geophys. Res.*, *116*, A12205, doi:10.1029/2011JA017035.

Li, W., J. Bortnik, R. M. Thorne, Y. Nishimura, V. Angelopoulos, and L. Chen (2011b), Modulation of whistler mode chorus waves: 2. Role of density variations, *J. Geophys. Res.*, *116*, A06206, doi:10.1029/2010JA016313.

Li, W., R. M. Thorne, J. Bortnik, Y. Nishimura, and V. Angelopoulos (2011c), Modulation of whistler mode chorus waves: 1. Role of compressional Pc4–5 pulsations, *J. Geophys. Res.*, *116*, A06205, doi:10.1029/2010JA016312.

Lorentzen, K. R., J. B. Blake, U. S. Inan, and J. Bortnik (2001), Observations of relativistic electron microbursts in association with VLF chorus, *J. Geophys. Res.*, *106*(A4), 6017–6027, doi:10.1029/2000JA003018.

Macúšová, E., et al. (2010), Observations of the relationship between frequency sweep rates of chorus wave packets and plasma density, *J. Geophys. Res.*, *115*, A12257, doi:10.1029/2010JA015468.

Manninen, J., N. G. Kleimenova, O. V. Kozyreva, and T. Turunen (2010), Pc5 geomagnetic pulsations, pulsating particle precipitation, and VLF chorus: Case study on 24 November 2006, *J. Geophys. Res.*, *115*, A00F14, doi:10.1029/2009JA014837.

McFadden, J. P., C. W. Carlson, D. Larson, M. Ludlam, R. Abiad, B. Elliott, P. Turin, M. Marckwordt, and V. Angelopoulos (2008), The THEMIS ESA plasma instrument and in-flight calibration, *Space Sci. Rev.*, *141*(1–4), 277–302, doi:10.1007/s11214-008-9440-2.

Means, J. D. (1972), Use of the three-dimension covariance matrix in analyzing the polarization properties of plane waves, *J. Geophys. Res.*, *77*(28), 5551–5559, doi:10.1029/JA077i028p05551.

Mende, S. B., H. U. Frey, J. McFadden, C. W. Carlson, V. Angelopoulos, K. H. Glassmeier, D. G. Sibeck, and A. Weatherwax (2009), Coordinated observation of the dayside magnetospheric entry and exit of the THEMIS satellites with ground-based auroral imaging in Antarctica, *J. Geophys. Res.*, *114*, A00C23, doi:10.1029/2008JA013496. [Printed *115*(A1), 2010.]

Meredith, N. P., R. B. Horne, A. D. Johnstone, and R. R. Anderson (2000), The temporal evolution of electron distributions and associated wave activity following substorm injections in the inner magnetosphere, *J. Geophys. Res.*, *105*(A6), 12,907–12,917, doi:10.1029/2000JA900010.

Meredith, N. P., R. B. Horne, and R. R. Anderson (2001a), Substorm dependence of chorus amplitudes: Implications for the acceleration of electrons to relativistic energies, *J. Geophys. Res.*, *106*(A7), 13,165–13,178, doi:10.1029/2000JA900156.

Meredith, N. P., R. B. Horne, and R. R. Anderson (2001b), Substorm dependence of chorus amplitudes: Implications for the acceleration of electrons to relativistic energies, *J. Geophys. Res.*, *106*(A7), 13,165–13,178, doi:10.1029/2000JA900156.

Meredith, N. P., R. B. Horne, R. M. Thorne, and R. R. Anderson (2009), Survey of upper band chorus and ECH waves: Implications for the diffuse aurora, *J. Geophys. Res.*, *114*, A07218, doi:10.1029/2009JA014230.

Millan, R. M., and R. M. Thorne (2007), Review of radiation belt relativistic electron losses, *J. Atmos. Sol. Terr. Phys.*, *69*(3), 362–377, doi:10.1016/j.jastp.2006.06.019.

Min, K., J. Lee, and K. Keika (2010), Chorus wave generation near the dawnside magnetopause due to drift shell splitting of substorm-injected electrons, *J. Geophys. Res.*, *115*, A00I02, doi:10.1029/2010JA015474. [Printed *116*(A5), 2011.]

Miyoshi, Y., A. Morioka, T. Obara, H. Misawa, T. Nagai, and Y. Kasahara (2003), Rebuilding process of the outer radiation belt during the 3 November 1993 magnetic storm: NOAA and Exos-D observations, *J. Geophys. Res.*, *108*(A1), 1004, doi:10.1029/2001JA007542.

Miyoshi, Y., A. Morioka, R. Kataoka, Y. Kasahara, and T. Mukai (2007), Evolution of the outer radiation belt during the November 1993 storms driven by corotating interaction regions, *J. Geophys. Res.*, *112*, A05210, doi:10.1029/2006JA012148.

Mozer, F. S. (1973), Analyses of techniques for measuring DC and AC electric fields in the magnetosphere, *Space Sci. Rev.*, *14*(2), 272–313, doi:10.1007/BF02432099.

Nosé, M., T. Iyemori, M. Sugiura, J. A. Slavin, R. A. Hoffman, J. D. Winningham, and N. Sato (1998), Electron precipitation accompanying Pc 5 pulsations observed by the DE satellites and at a ground station, *J. Geophys. Res.*, *103*(A8), 17,587–17,604, doi:10.1029/98JA01187.

Nunn, D. (1974), A self-consistent theory of triggered VLF emissions, *Planet. Space Sci.*, *22*(3), 349–378, doi:10.1016/0032-0633(74)90070-1.

Omura, Y., and D. Nunn (2011), Triggering process of whistler mode chorus emissions in the magnetosphere, *J. Geophys. Res.*, *116*, A05205, doi:10.1029/2010JA016280.

Omura, Y., D. Nunn, H. Matsumoto, and M. J. Rycroft (1991), A review of observational, theoretical and numerical studies of VLF triggered emissions, *J. Atmos. Terr. Phys.*, *53*(5), 351–368, doi:10.1016/0021-9169(91)90031-2.

Omura, Y., Y. Katoh, and D. Summers (2008), Theory and simulation of the generation of whistler-mode chorus, *J. Geophys. Res.*, *113*, A04223, doi:10.1029/2007JA012622.

Omura, Y., M. Hikishima, Y. Katoh, D. Summers, and S. Yagitani (2009), Nonlinear mechanisms of lower-band and upper-band VLF chorus emissions in the magnetosphere, *J. Geophys. Res.*, *114*, A07217, doi:10.1029/2009JA014206.

Öztürk, M. K., and R. A. Wolf (2007), Bifurcation of drift shells near the dayside magnetopause, *J. Geophys. Res.*, *112*, A07207, doi:10.1029/2006JA012102.

Parrot, M., O. Santolík, N. Cornilleau-Wehrlin, M. Maksimovic, and C. C. Harvery (2003a), Source location of chorus emissions observed by Cluster, *Ann. Geophys.*, *21*(2), 473–480, doi:10.5194/angeo-21-473-2003.

Parrot, M., O. Santolík, N. Cornilleau-Wehrlin, M. Maksimovic, and C. Harvery (2003b), Magnetospherically reflected chorus waves revealed by ray tracing with CLUSTER data, *Ann. Geophys.*, *21*(5), 1111–1120, doi:10.5194/angeo-21-1111-2003.

Pedersen, A., F. Mozer, and G. Gustafsson (1998), Electric field measurements in a tenuous plasma with spherical double probes, in *Measurement Techniques in Space Plasmas: Fields*, *Geophys. Monogr. Ser.*, vol. 103, edited by F. Pfaff, E. Borovsky, and T. Young, pp. 1–12, AGU, Washington, D. C., doi:10.1029/GM103p0001.

Roederer, J. G. (1967), On the adiabatic motion of energetic particles in a model magnetosphere, *J. Geophys. Res.*, *72*(3), 981–992, doi:10.1029/JZ072i003p00981.

Roederer, J. G. (1970), *Dynamics of Geomagnetically Trapped Radiation*, Springer, New York, doi:10.1007/978-3-642-49300-3.

Roux, A., O. Le Contel, C. Coillot, A. Bouabdellah, B. Porte, D. Alison, S. Ruocco, and M. C. Vassal (2008), The search coil magnetometer for

THEMIS, *Space Sci. Rev.*, *141*(1–4), 265–275, doi:10.1007/s11214-008-9455-8.

Saito, S., Y. Miyoshi, and K. Seki (2010), A split in the outer radiation belt by magnetopausse shadowing: Test particle simulations, *J. Geophys. Res.*, *115*, A08210, doi:10.1029/2009JA014738.

Salvati, M. A., U. S. Inan, T. J. Rosenberg, and A. T. Weatherwax (2000), Solar wind control of polar chorus, *J. Geophys. Res.*, *27*(5), 649–652.

Santolík, O., et al. (2010a), Wave-particle interactions in the equatorial source region of whistler-mode emissions, *J. Geophys. Res.*, *115*, A00F16, doi:10.1029/2009JA015218.

Santolík, O., J. S. Pickett, D. A. Gurnett, J. D. Menietti, B. T. Tsurutani, and O. Verkhoglyadova (2010b), Survey of Poynting flux of whistler mode chorus in the outer zone, *J. Geophys. Res.*, *115*, A00F13, doi:10.1029/2009JA014925.

Sarris, T. E., T. M. Loto'aniu, X. Li, and J. Singer (2007), Observations at geosynchronous orbit of a persistent Pc5 geomagnetic pulsation and energetic electron flux modulations, *Ann. Geophys.*, *25*, 1653–1667, doi:10.5194/angeo-25-1653-2007.

Sazhin, S. S., and M. Hayakawa (1992), Magnetospheric chorus emissions: A review, *Planet. Space Sci.*, *40*(5), 681–697, doi:10.1016/0032-0633(92)90009-D.

Schriver, D., et al. (2010), Generation of whistler mode emissions in the inner magnetosphere: An event study, *J. Geophys. Res.*, *115*, A00F17, doi:10.1029/2009JA014932.

Schulz, M., and L. J. Lanzerotti (1974), *Particle Diffusion in the Radiation Belts*, Springer, New York, doi:10.1007/978-3-642-65675-0.

Shabansky, V. P. (1971), Some processes in the magnetosphere, *Space Sci. Rev.*, *12*, 299–418, doi:10.1007/BF00165511.

Sheeley, B. W., M. B. Moldwin, H. K. Rassoul, and R. R. Anderson (2001), An empirical plasmasphere and trough density model: CRRES observations, *J. Geophys. Res.*, *106*(A11), 25,631–25,641, doi:10.1029/2000JA000286.

Shprits, Y. Y., N. P. Meredith, and R. M. Thorne (2007), Parameterization of radiation belt electron loss timescales due to interactions with chorus waves, *Geophys. Res. Lett.*, *34*, L11110, doi:10.1029/2006GL029050.

Sibeck, D. G., R. W. McEntire, A. T. Y. Lui, R. E. Lopez, and S. M. Krimigis (1987), Magnetic field drift shell splitting: Cause of unusual dayside particle pitch angle distributions during storms and substorms, *J. Geophys. Res.*, *92*(A12), 13,458–13,497, doi:10.1029/JA092iA12p13485.

Sigsbee, K., J. D. Menietti, O. Santolík, and J. S. Pickett (2010), Locations of chorus emissions observed by the Polar Plasma Wave Instrument, *J. Geophys. Res.*, *115*, A00F12, doi:10.1029/2009JA014579.

Spanswick, E., E. Donovan, and G. Baker (2005), Pc5 modulation of high energy electron precipitation: Particle interaction regions and scattering efficiency, *Ann. Geophys.*, *23*, 1533–1542, doi:10.5194/angeo-23-1533-2005.

Spasojević, M., and U. S. Inan (2010), Drivers of chorus in the outer dayside magnetosphere, *J. Geophys. Res.*, *115*, A00F09, doi:10.1029/2009JA014452.

Su, Z., H. Zheng, and S. Wang (2009), Evolution of electron pitch angle distribution due to interactions with whistler mode chorus following substorm injections, *J. Geophys. Res.*, *114*, A08202, doi:10.1029/2009JA014269.

Summers, D., B. Ni, and N. P. Meredith (2007), Timescales for radiation belt electron acceleration and loss due to resonant wave-particle interactions: 2. Evaluation for VLF chorus, ELF hiss, and electromagnetic ion cyclotron waves, *J. Geophys. Res.*, *112*, A04207, doi:10.1029/2006JA011993.

Takahashi, K., B. J. Anderson, S.-I. Ohtani, G. D. Reeves, S. Takahashi, T. E. Sarris, and K. Mursula (1997), Drift-shell splitting of energetic ions injected at pseudo-substorm onsets, *J. Geophys. Res.*, *102*(A10), 22,117–22,130, doi:10.1029/97JA01870.

Tao, X., R. M. Thorne, W. Li, B. Ni, N. P. Meredith, and R. B. Horne (2011), Evolution of electron pitch angle distributions following injection from the plasma sheet, *J. Geophys. Res.*, *116*, A04229, doi:10.1029/2010JA016245.

Thorne, R. M., B. Ni, X. Tao, R. B. Horne, and N. P. Meredith (2010), Scattering by chorus waves as the dominant cause of diffuse auroral precipitation, *Nature*, *467*(7318), 943–946, doi:10.1038/nature09467.

Tsurutani, B. T., and E. J. Smith (1974), Postmidnight chorus: A substorm phenomenon, *J. Geophys. Res.*, *79*(1), 118–127, doi:10.1029/JA079i001p00118.

Tsurutani, B. T., and E. J. Smith (1977), Two types of magnetospheric ELF chorus and their substorm dependences, *J. Geophys. Res.*, *82*(32), 5112–5128, doi:10.1029/JA082i032p05112.

Tsurutani, B. T., O. P. Verkhoglyadova, G. S. Lakhina, and S. Yagitani (2009), Properties of dayside outer zone chorus during HILDCAA events: Loss of energetic electrons, *J. Geophys. Res.*, *114*, A03207, doi:10.1029/2008JA013353.

Tsyganenko, N. A. (2002a), A model of the near magnetosphere with a dawn-dusk asymmetry: 1. Mathematical structure, *J. Geophys. Res.*, *107*(A8), 1179, doi:10.1029/2001JA000219.

Tsyganenko, N. A. (2002b), A model of the near magnetosphere with a dawn-dusk asymmetry: 2. Parameterization and fitting to observations, *J. Geophys. Res.*, *107*(A8), 1176, doi:10.1029/2001JA000220.

Ukhorskiy, A. Y., M. I. Sitnov, R. M. Millan, and B. T. Kress (2011), The role of drift orbit bifurcations in energization and loss of electrons in the outer radiation belt, *J. Geophys. Res.*, *116*, A09208, doi:10.1029/2011JA016623.

Vaivads, A., O. Santolík, G. Stenberg, M. André, C. J. Owen, P. Canu, and M. Dunlop (2007), Source of whistler emissions at the dayside magnetopause, *Geophys. Res. Lett.*, *34*, L09106, doi:10.1029/2006GL029195.

West, H. I., R. M. Buck, and J. R. Walton (1973), Electron pitch angle distributions throughout the magnetosphere as observed on Ogo 5, *J. Geophys. Res.*, *78*(7), 1064–1081, doi:10.1029/JA078i007p01064.

Wrenn, G. L., J. F. E. Johnson, and J. J. Sojka (1979), Stable "pancake" distributions of low energy electrons in the plasma trough, *Nature*, *279*(5713), 512–514, doi:10.1038/279512a0.